Experimental Thermal and Fluid Science 76 (2016) 175–184

Contents lists available at ScienceDirect

Experimental Thermal and Fluid Science

journal homepage: www.elsevier.com/locate/etfs

Transition from stratified to non-stratified oil–water flows using a bluff body

K.H. Park, M. Chinaud, P. Angeli *

Department of Chemical Engineering, University College London, London WC1E 7JE, UK

ARTICLE INFO

Article history:
Received 15 November 2015
Received in revised form 11 February 2016
Accepted 17 March 2016
Available online 21 March 2016

Keywords:
Oil–water flow
Bluff body
Stratified flow
Non-stratified flow

ABSTRACT

In this paper the effect of a transverse cylindrical rod immersed in water on the flow patterns and interfacial characteristics of an oil–water pipe flow is investigated experimentally. The cylinder is used to passively actuate the transition from stratified to non-stratified flows and to localise the formation of waves and the detachment of drops. The studies are carried out in an acrylic test section with 37 mm ID using as test fluids tap water and Exxsol D140 (density 830 kg m^{-3} and viscosity 5.5 cP). The rod has 5 mm diameter and is located at 460 mm from the test section inlet. Flow patterns and interface characteristics were studied with high speed imaging. It was found that the presence of the rod generates waves shortly downstream, from which drops detach, and reduces the mixture velocity for the transition from stratified to non-stratified flows. The average interface height and wave amplitude increase with distance from the rod, while the average wave length and frequency remain almost constant. The Strouhal number is found to be equal to 0.24, while the wave velocities are slightly higher than the mixture velocities.

1. Introduction

The simultaneous flow of two immiscible liquids inside a pipe is commonly encountered in many applications including transportation in the petroleum industry, emulsifications and two-phase reactions and separations in the process industries. The transport phenomena in such flows depend on the flow configurations, while models have been developed to predict the transitions between different flow patterns [1–7]. The transition from stratified flows, in particular, has received a lot of interest. In liquid–liquid flows this transition leads to dispersed patterns and is considered to happen when, with increasing flowrates, waves develop at the oil–water interface in stratified flows from which drops detach [8]. However, there is still a lack of experimental data on the development of waves and their characteristics in liquid–liquid pipe flows, especially near the transition boundaries from stratified to non-stratified regimes. This is partly because experimentally it is very difficult to localise the droplet detachment events and to investigate the characteristics of the breaking waves. The physical mechanism behind the transition from stratified to non-stratified flows is, therefore, yet to be fully understood.

A small number of studies have been carried out on the stability of waves in stratified flows in terms of different flow parameters [9,1,2,8,10] while a number of studies have focused on interfacial waves in annular flows [11–16]. Only recently Al-Wahaibi and Angeli [17] investigated the interfacial wave characteristics during the transition from stratified to non-stratified flows using a double-wire conductance probe. They reported that interfacial waves must be present for drops to appear and the characteristics of the waves are a function of the mixture velocity and the ratio of the velocities of the two phases. The results were later confirmed by Barral et al. [18] who also used a conductance probe and high speed imaging to obtain interfacial wave characteristics. In both studies, the exact axial location in the pipe where drops detach and the transition from stratified to non-stratified flows was not identified.

In this work, a novel approach is followed to facilitate the study of interfacial waves and of drop detachment, which is based on the use of a bluff body located close to the oil–water interface. The bluff body passively actuates the formation of waves and the transition from stratified to non-stratified flows. The idea was inspired from previous studies where hydrofoils have been used to increase air entrainment in water and reduce frictional drag around ships [19,20]. A cylindrical rod is adopted as a bluff body in the current investigations and this approach is applied for the first time to cause and localise drop formation in liquid–liquid pipe flows.

The flow around cylinders in single phase flows has been studied extensively (reviews are given by Berger and Wille [21]; Lin and Pao [22]; Bearman [23]; Oertel [24]; Griffin and Hall [25];

* Corresponding author.
E-mail address: p.angeli@ucl.ac.uk (P. Angeli).

http://dx.doi.org/10.1016/j.expthermflusci.2016.03.017
0894-1777/

Coutanceau and Defaye [26]; Williamson [27,28]; Zdravkovich [29]) and these flows are mainly characterised by two dimensionless numbers, the cylinder based *Reynolds number* and the *Strouhal number* which can be written as follows:

$$Re = \frac{\rho U_w D_{rod}}{\mu} \quad (1)$$

$$St = \frac{f D_{rod}}{U_w} = \frac{\rho D_{rod}^2}{\mu} \frac{f}{Re} \quad (2)$$

where ρ, μ, u_w and D_{rod} are the density, viscosity, velocity of the fluid and diameter of the rod respectively and f is the frequency of the dominant vortex shed behind the bluff body. At very low Reynolds numbers ($Re < 5$) the flow is highly viscous hence there are no vortices generated. As the fluid velocity increases ($Re > 46$) von Karman vortices are generated. All flow conditions investigated near the wake of the bluff body in the present study are above Re_c, which is the critical Reynolds number where the first vortex shedding is observed. The Strouhal number gives a measure of the predominant shedding frequency of the vortices and for an unbounded single phase flow around a smooth cylinder it is about 0.2.

A few studies have investigated the interactions between a free surface and vortices shed by bluff bodies of different shapes. Hydrofoils are commonly used in these studies because of their relevance to marine applications. Duncan [19] used a hydrofoil towed inside a deep water channel to generate breaking waves. Surface depression was observed just behind the bluff body while the wavelength and the crest-to-trough amplitude were proportional to the hydrofoil speed squared. Lin and Rockwell [30] studied the free surface shape and breaking waves downstream a hydrofoil and obtained velocity profiles using Particle Image Velocimetry (PIV). They observed a sharp elevation of the interface just behind the bluff body which increased with increasing Froude number ($Fr = u/\sqrt{gd}$, where g, d and u are the gravitational force, foil chord length and free stream velocity respectively). Square shaped bluff bodies have also been studied as they are relevant to architectural and engineering applications in the design of buildings and bridges. Malavaski and Guadagnini [31–33] observed free surface distortion when a square cylinder was submerged in a water channel at various distances above the channel wall. They also suggested proximity of the bluff body to the free surface was responsible for the change in drag and lift coefficients that depended on the Reynolds number.

A number of studies have been carried out using cylinders as bluff bodies because of their simplicity. Miyata et al. [34] conducted both experimental and numerical investigations using a cylinder near a free water surface. Only one flow condition was investigated at various depths of submergence (h/D_{rod}; where h is the distance between the free surface and the top of the bluff body), and no surface distortion was observed. However, different wake states were apparent from visual observations made using tracer particles illuminated and then captured with long exposure time (0.5 s). The wake states were interpreted in terms of corresponding drag and lift forces measured with a load cell attached to a cylinder. Similar wake states were later observed by Sheridan et al. [35] who used PIV to study the vortices generated downstream the cylinder in a deep water channel at various distances from the free water surface. The wake states were related to Fr and h/D_{rod} while large surface distortion was observed only at certain Fr and h/D_{rod}. Experimental investigations by Carberry et al. [36,37] and numerical studies by Reichl et al. [38] produced similar results. In all cases where a free surface was disturbed, a jet-like flow was generated from the top of the bluff body which moved towards the free surface and caused the formation of waves. In these studies the Froude number varied between 0.166 and 0.97.

The effect of a wall on the flow characteristics at the wake of a cylinder has been studied mainly in two dimensional configurations and single phase flows with a single flat boundary. The presence of a wall close to the cylinder was found to suppress vortex formation for gap ratios, H/D_{rod} (where H is the distance between the rod and the wall) less than 0.3–0.4 [39–46]. The frequency of the dominant vortex shed has been found to increase with increasing Re once vortex shedding has been established but the Strouhal number remained constant at 0.2. Grass et al. [42] on the other hand reported that the Strouhal number tends to increase as H/D_{rod} decreases with a maximum increase of 10%. Price et al. [45] also found that St can be as high as 0.4 when H/D_{rod} is 0.25.

There are currently no experimental or theoretical studies which look at the effect of bluff bodies on flow inside pipes, in either single or two phase flows. The current work investigates the effect of a cylinder immersed in the water phase of a two-phase oil–water pipe flow on the interface characteristics, using high speed imaging and conductance probes. The main objective is to passively actuate waves at the oil–water interface and to localise the formation of droplets. In this study, for the first time the combined interactions of a bluff body with a wall and an interface are considered.

2. Experimental set up and methods

The studies were carried out in the oil–water flow facility located in the Multiphase Flow Lab, Department of Chemical Engineering, UCL (see Fig. 1). The two test fluids used are Exxsol D140 oil and tap water with properties given in Table 1. The two fluids are stored separately in tanks and are led via separate pumps into the test section. Their flowrates are regulated via gate valves and measured separately with variable area flow meters (ABB Instrumentation Ltd) with a range from 20 L/min to 240 L/min and accuracy of 1% full scale. The inlet of the test section is a symmetrical Y-shaped junction with 20° angle (Fig. 1), which allows the fluids to enter according to their density with minimal mixing. The test section is an 8 m long acrylic pipe with 37 mm ID. After the test section the two-phase mixture returns to a separator vessel equipped with a KnitMesh™ coalescer that facilitates the separation; the separated fluids then flow by gravity back to their respective tanks.

2.1. Bluff body design

A pipe section housing the fixed bluff body was designed and manufactured in-house (Fig. 2). The pipe section was made from acrylic with 2 flanges attached at each end that connect it to the rest of the test section. A cylindrical acrylic rod has been chosen as the first bluff body design to be studied. The rod has 5 mm OD and is positioned perpendicularly to the fluid flow at 9.25 mm below the pipe centre line, equivalent to a quarter of the pipe diameter (Fig. 2). The rod diameter and vertical position were chosen based on available studies similar to the current work considering 3 main parameters, H/D_{rod}, h/D_{rod} and the blockage ratio (ratio between the cylinder diameter and the pipe diameter). In the present study, the gap between the rod and the bottom wall, H/D_{rod}, is 1.35 and does not obstruct the formation of von Karman vortices; this value is largely above the critical H/D_{rod} of 0.3–0.4 as discussed previously. In addition, the current rod position leaves sufficient distance between the rod and the top wall and therefore allows a range of interface heights (and phase flowrates) to be investigated without a direct impact of the interface on the cylinder. The blockage ratio for the current study is 0.13 and was chosen based on the study by Chen et al. [47] who found no significant impact on the flow for blockage ratios below 0.5. As the bluff body has a fixed position, the distance between the cylinder and the

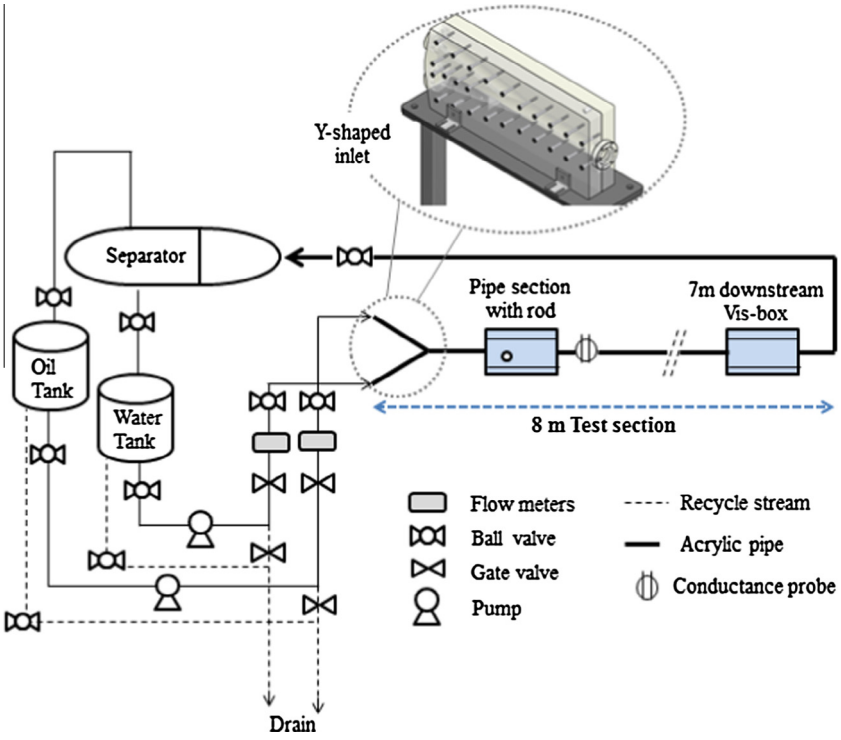

Fig. 1. Schematic diagram of the two phase flow facility and the symmetrical Y-shaped inlet.

Table 1
Properties of the test fluids.

	Exxsol D140	Water
Density, kg/m^3 @ 25 °C	830	1000
Viscosity, cP, @ 25 °C	5.5	1
Interfacial tension mN/m @ 25 °C	39.6	

interface can only be varied by changing the input phase flow rates. During the experiments, the pipe section with the rod is installed next to the symmetrical Y-inlet giving a distance between the inlet and the rod of approximately 460 mm. This distance was chosen taking into account two main considerations. Placing the rod close to the inlet allows maximum downstream test section length for the studies of wave and drop formation and flow pattern changes. Previous single phase PIV results showed that the flow was already fully developed at this distance. In addition, it was found that Kelvin–Helmholtz waves forming after the inlet are mainly smooth and two dimensional for a short distance but then develop 3D fluctuations. Positioning the rod close to the inlet ensured that only smooth waves would interact with the rod; such waves are more easy to implement as initial conditions in numerical simulations of these flows that will be used to compare in the future against the experimental data.

The flow patterns downstream the bluff body were recorded with a high speed camera (Photron SA-1; resolution 1024 × 1024 pixels). A movable visualisation box filled with glycerol, which has refractive index similar to the pipe material, was installed around the test section at the position of the recording to minimise optical distortions. Recording speeds between 1 and 2 kHz were used depending on the flowrates. Experiments were conducted for mixture velocities ranging between 0.62 and 2.17 m/s and oil-to-water flow rate ratios, r, between 0.29 and 3.5.

Interfacial wave characteristics were obtained from the high speed images and a double-wire conductivity probe. The probe was made in-house and consists of two stainless steel wires, 0.5 mm in diameter, 5 mm apart, installed perpendicularly to the direction of the flow. The two wires form part of an electrical resistance circuit whose signal depends on the height of the water layer between the two wires in separated oil–water flows. The signal gives the variation of the interface height with time at this particular axial location in the pipe. This type of probe has been used widely in gas–liquid and liquid–liquid flows to investigate interfacial waves [48–53,18]. Data was collected at 256 Hz over a period of 4 min for two-phase flows. Single phase water measurements

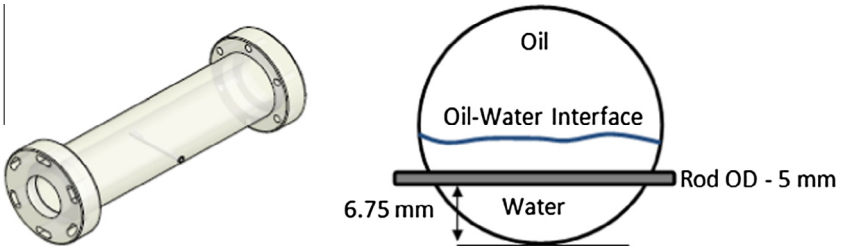

Fig. 2. 3D and schematic drawing of the pipe section with the rod.

were also carried out to account for any variations in the conductivity of the water phase. The data collection and the processing methodology have been described in Barral et al. [18]. The probe was located just after the bluff body (19D) to study interfacial waves generated by the rod. The probe signal represents the interface height reliably only when there are no or very few drops of one phase into the other which limits the range of flow rates it can be used.

Wave characteristics were also acquired from the high speed images. In each image several measuring locations were chosen at fixed distance from the rod and equally spaced apart, as shown in Fig. 3. The fixed locations were 40, 55.9, 71.8, 87.7 and 103.6 mm away from the rod. To calculate the *local average interface height* at each measuring location the height of the interface is recorded in pixels every 10 ms for 1.5 s. For each measuring location the data acquired are averaged to obtain the local interface height. Similarly, given the local average interface height, the *local average wave amplitudes* are calculated by subtracting the local average interface height from individual wave crest positions, which are then averaged. To calculate the *local average wave velocity* individual wave crests were tracked in the direction of flow and the time taken for each crest to travel past each measuring location was recorded. The wave velocities were then averaged to obtain local average wave velocity per measuring location. The time difference between two successive crests or troughs passing through a measuring location was also recorded. Knowing the average wave velocity, the *local average wavelength* could be computed from the time a pair of crests or troughs needed to travel past each measuring point. *Wave frequencies* were also computed from the number of wave crests and troughs travelled past the measuring locations. During the above calculations, the main source of uncertainty arises during the data extraction process from the high speed images. The uncertainty is estimated to a maximum of 5 pixels (0.16 mm/pixel) or 0.8 mm, which is equivalent to the apparent thickness of the interface on the images.

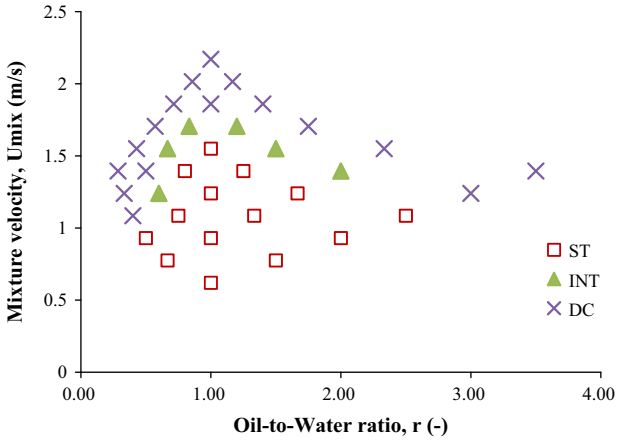

Fig. 4. Flow pattern map at 7 m downstream the inlet when there is no bluff body installed.

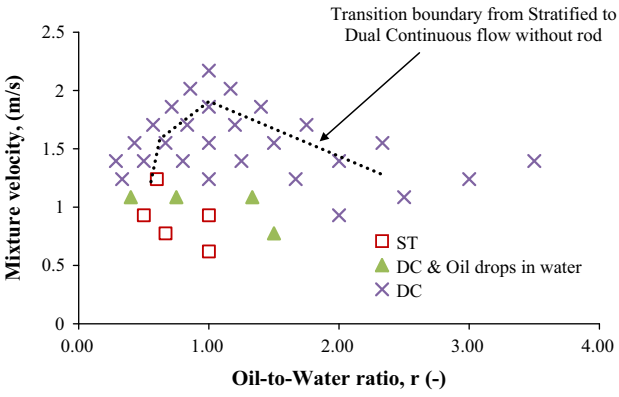

Fig. 5. Flow pattern map at 7 m downstream the inlet with the bluff body installed.

3. Experimental results

3.1. Flow patterns at 7 m downstream the inlet

Flow patterns were observed in both cases without and with the bluff body with the high speed camera at 7 m downstream the inlet (189D). Experiments were carried out for mixture velocities between 0.62 and 2.17 m/s and input oil-to-water flow rate ratios between 0.29 and 3.5. The flow patterns identified in both cases are plotted in Figs. 4 and 5 in terms of mixture velocity, U_{mix}, against oil to water input flowrate ratio, r. Three different flow patterns were observed in both systems with and without the bluff body installed. The patterns when no bluff body (Fig. 4) was present showed good agreement with patterns identified in previous studies in the same system [54]. The intermediate, INT, pattern was only observed in the system without the rod, (r range between 0.5 and 2.5 and U_{mix} range between 0.62 and 1.55) while stratified, ST, and dual continuous, DC, flows appeared in both systems. In the system with the bluff body, a new pattern was seen, dual continuous flow with oil drops in water only, DC & Oil drops in water.

The transition from stratified to non-stratified flows occurs with increasing mixture velocity in both cases. The transition was considered to have taken place when a droplet of either oil or water first appears. This transition is delayed to higher mixture velocities

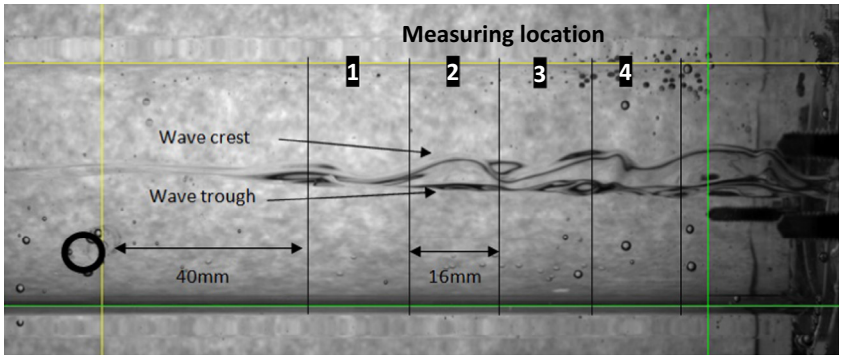

Fig. 3. Image of waves generated behind the bluff body (U_{mix} = 0.62 m/s, r = 1). The locations used in the wave analysis are shown.

at flow rate ratios around 1, where the relative velocities between the two phases are low, in agreement with previous work [54]. The presence of the bluff body reduces the region of stratified flow significantly (see Fig. 5). The transition boundary with the bluff body is found at a much narrower range of r between 0.4 and 1.5 and U_{mix} between 0.62 and 1.09 m/s compared to the transition boundary without the rod (dotted line shown in Fig. 5). This suggests that the rod actuates the transition between the patterns.

3.1.1. Stratified flows (ST)

Stratified flow with smooth interface was only observed when there was no cylinder at the lowest mixture velocity studied, U_{mix} = 0.62 m/s, and equal phase flowrates (see Fig. 6a). For the same flow condition small fluctuations of the interface were observed at 7 m from the inlet with the addition of the bluff body. In general, at low velocities waves formed after the inlet decayed downstream. Barral et al. [18] in flows without a bluff body, also found that waves gradually fade with distance. With increasing mixture velocity in both cases with and without bluff body, the waves persist in the downstream location. Fig. 6b shows stratified (ST) flows for the two systems at higher mixture velocities (U_{mix} = 0.78 m/s, r = 0.67). As can be seen, the interfacial waves are more prominent when the bluff body is present.

3.1.2. Dual continuous flow (DC)

In this pattern both oil and water retain their continuity at the top and the bottom of the pipe respectively while drops of one phase appear into the other. The degree of dispersion depends on the mixture velocity and the phase flowrate ratio. This regime appeared in both systems at high mixture velocities. As the velocities increased the drop size decreased. When the rod was present, for the same flow conditions, more drops appeared in the phases as can be seen in Fig. 6c. For similar mixture velocities, drops are larger and of similar size in the case of small input ratios ($r \leqslant 1$), while they are generally smaller with variable sizes at large input ratios ($r \geqslant 2$). Barral et al. [55] also observed qualitative difference in the average droplet size in the dual continuous regime between low and high input flowrate ratios.

A particular case of the dual continuous pattern is the *Dual continuous flow with oil drops in water (DC & Oil drops in water),* where

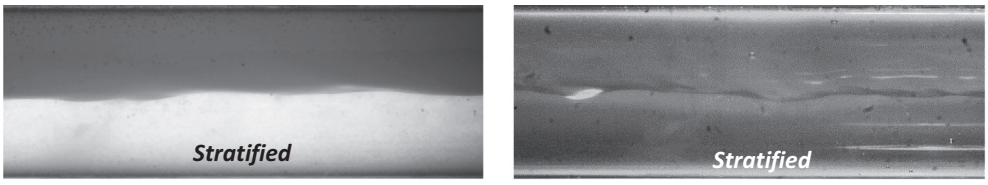

(a) Umix = 0.62 m/s, r = 1

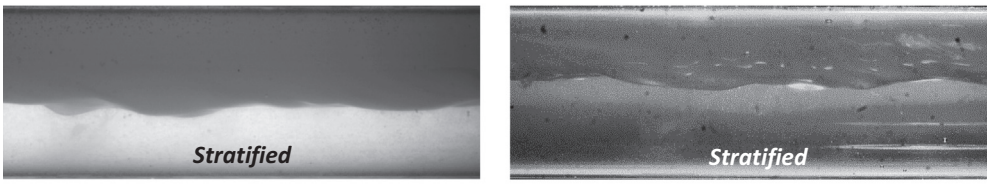

(b) Umix = 0.78 m/s, r = 0.67

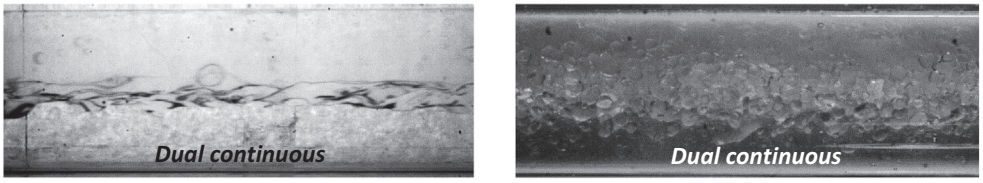

(c) Umix = 1.86 m/s, r = 1

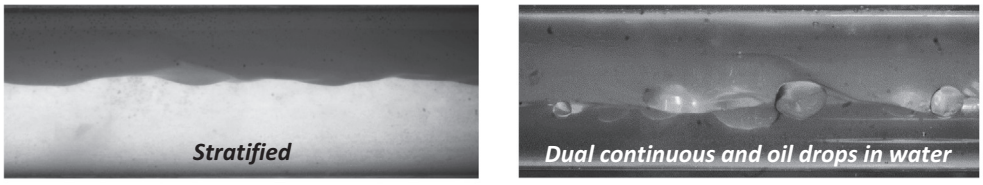

(d) Umix = 0.78 m/s, r = 1.50

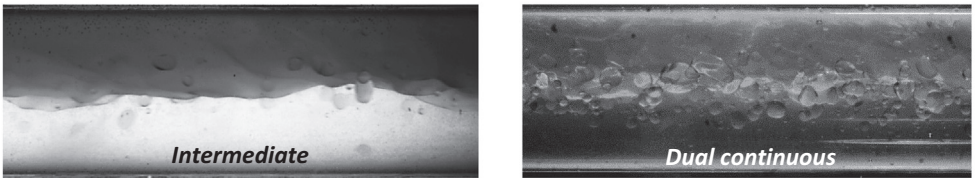

(e) Umix = 1.71 m/s, r = 0.83

Fig. 6. Flow patterns at 7 m downstream the inlet without (left) and with (right) rod present.

only oil drops appeared in the water phase. This flow regime was only observed in the system with the bluff body in place for a narrow range of U_{mix} (1.09–0.78 m/s) and input ratios (1.5–0.4) (Fig. 6d). The oil drops are large compared to the other DC cases. The overall shape of the interface appeared wavy but the wave surfaces were rather smooth which suggests that the drops found at these flow conditions must have been formed upstream (i.e. behind the bluff body). For the same flow conditions in the system without the bluff body the flows were stratified wavy.

3.1.3. Intermediate flow

This regime was only observed in the system without the bluff body, between stratified and dual continuous flows. It is characterised by continuous phases of oil and water with fluctuating interface and the appearance of small sporadic drops in the two phases. The size of the droplets is smaller than in the DC regime. Mixture velocity and input flowrate ratio did not affect significantly the appearance of the interface. With the addition of the rod, under the same conditions, the flow was dual continuous (Fig. 6e).

3.2. Flow immediately downstream the bluff body

The visual observation of the flow patterns revealed that the rod had a significant effect on the flow which persisted 7 m downstream the inlet. This effect on the flow and the waves generated were studied immediately after the rod for mixture velocities ranging between 0.62 and 1.24 m/s and input flowrate ratio, *r*, varying between 0.67 and 1.5 (a total of 7 conditions). The flow conditions were chosen for two main reasons. Within this range, the interface did not directly impinge on the rod. In addition, for flow conditions outside this range, due to Kelvin–Helmholtz instability, waves with large amplitudes and 3D fluctuations form. For the limited conditions investigated, Kelvin–Helmholtz waves form after the inlet but they are mainly smooth over the short distance between the inlet and the rod. This allows only smooth waves to interact with the rod which would make modelling easier [56]. In addition, waves observed outside these flow conditions after the cylinder were strongly non-linear and difficult to analyse from the images. A total of 80 waves were extracted from the high speed images for each flow condition.

3.2.1. Average interface height

The average position of the interface, calculated from the images as discussed before, is plotted in Fig. 7 for all flow conditions studied. As can be seen, the mean interface position gradually increased with distance away from the bluff body. This increase is almost linear and, on average, the change is approximately 3 mm at the furthest distance of 104 mm from the rod.

The effect of mixture velocity on the average position of the interface is shown in Fig. 8 for the same flowrate ratio. Interestingly, higher mixture velocities resulted in larger interface heights. In addition, the height increased with distance from the rod at a rate which increases with mixture velocity. At 40 mm away from the rod, all three conditions have similar average interface height, (20.7, 21.1 and 22.1 mm) while at 104 mm away from the rod the average interface position has increased to 21.8, 23.8 and 25.5 mm respectively. The experimentally found interface heights at 40 mm downstream the rod were by an average of 1.3 mm higher than the interface heights found at a similar position when the rod was not present. For constant mixture velocity, the oil-to-water flowrate ratio affected the average interface height but did not affect significantly its rate of increase with distance from the rod (Fig. 9a and b).

The increase in interface height agrees with previous studies by Duncan [19] and Lin and Rockwell [30] where a sharp elevation of the interface was observed behind a hydrofoil submerged in water. The elevation was found to increase with increasing Froude number in agreement with the effect of mixture velocity on interface height in the current study.

3.2.2. Average wave amplitude and wave length

Wave amplitudes downstream the bluff body increased initially until they reached a plateau at approximately 72 mm while they slightly decreased in some cases at 104 mm (Fig. 10). Barral et al. [18] observed the opposite trend where the wave amplitudes decreased with distance, but the waves in that work were generated by KH instabilities only. The oil to water flowrate ratio was found to affect the wave amplitudes and their development, as can be seen in Fig. 11a and b. Larger wave amplitudes were obtained with the higher ratios. This is because at high r the interface height is low and close to the rod and can be more easily affected by the von Karman vortices shed by the bluff body within the water phase. Free surface distortions were also seen in previous studies [35,38] at specific Froude number-depth of submergence ratios (Fr = 0.35–0.60 and h/D_{rod} = 0.40, Fr = 0.72 and h/D_{rod} = 2.0, 1.18). The current studies have depth of submergence ratios h/D_{rod} = 1.04–2.21 and high Froude numbers Fr = 2.57–5.12 which will further affect the interface [57].

An increase in mixture velocity increased the wave amplitude at constant flowrate ratio (Fig. 12). On average, for an increase in mixture velocity from 0.62 to 0.93 m/s, the wave amplitude increased by about 50% (between 1 mm and 1.5 mm) at all distances away from the rod. For an increase in mixture velocity from 0.93 to 1.24 m/s, the difference between the average wave amplitudes increased with distance from the rod, with almost no difference between 40 mm and 56 mm and a difference of 0.6 mm at 104 mm away from the rod. At high mixture velocities the inter-

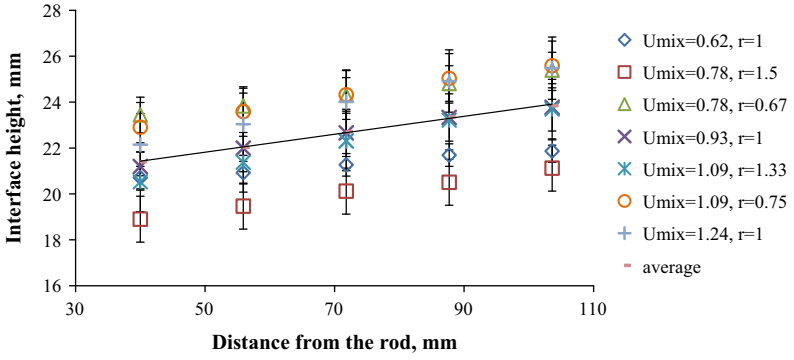

Fig. 7. Average interface height at different distances behind the bluff body for all flow conditions investigated.

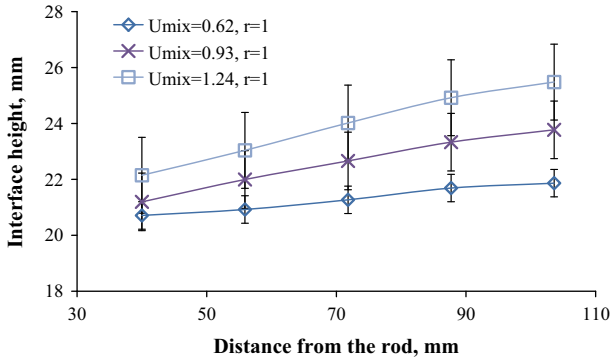

Fig. 8. Effect of mixture velocity on interface height at different distances from the bluff body for $r = 1$.

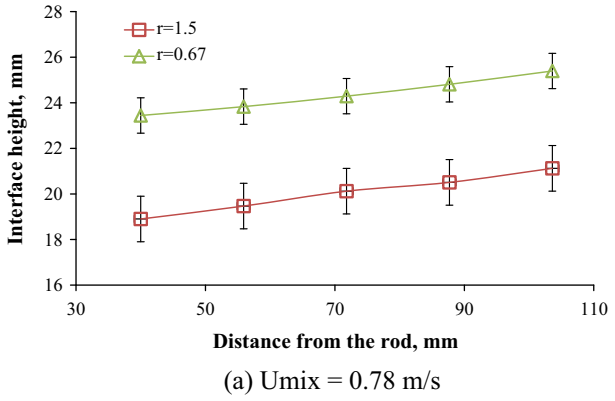

(a) Umix = 0.78 m/s

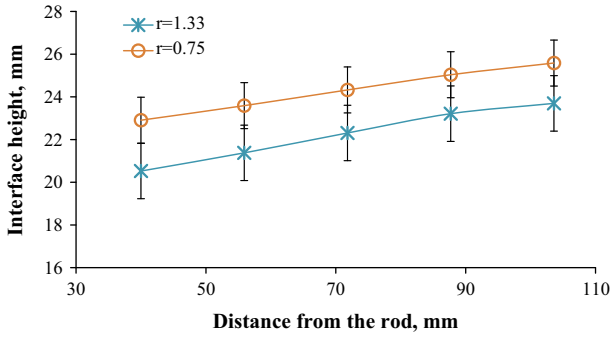

(b) Umix = 1.09 m/s

Fig. 9. Effect of input flow rate ratio on interface height at different distances from the bluff body.

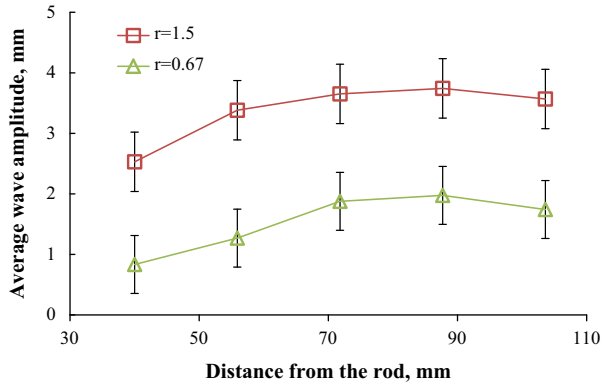

(a) Umix = 0.78 m/s

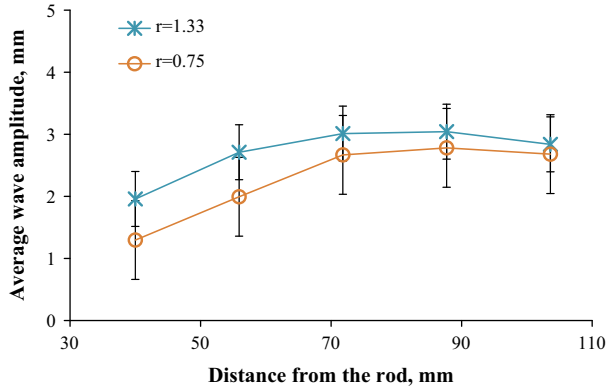

(b) Umix = 1.09 m/s

Fig. 11. Effect of input flow rate ratio on average wave amplitudes at different distances from the bluff body.

face height is slightly increased (Fig. 8) and the interactions between the rod and the interface should be decreased. However, the increase in mixture velocity is accompanied by increased water phase velocity past the rod. This would increase the magnitude of the von Karman vortices generated by the rod which affect the amplitude of the interfacial waves [35]. Dimas [57] also observed the change in the wave amplitude as Froude number increased and found that the shape of the free surface changed from sinusoidal to non-sinusoidal.

The average wavelengths did not vary significantly over distance until 72 mm away from the rod and then increased slightly further downstream by 0.5 mm on average (Fig. 13). The change

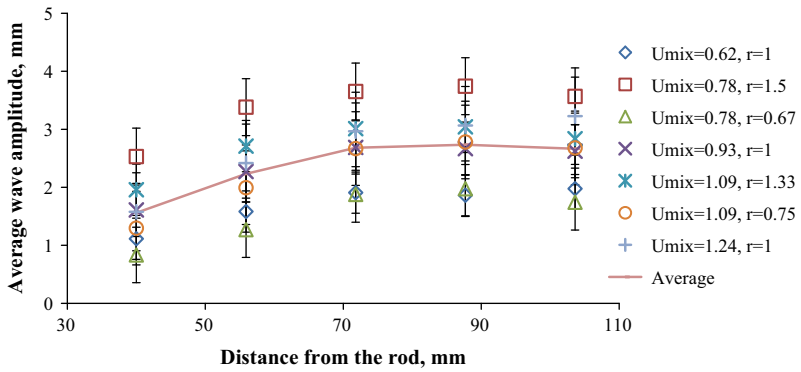

Fig. 10. Average wave amplitudes at different distances from the bluff body for all flow conditions investigated.

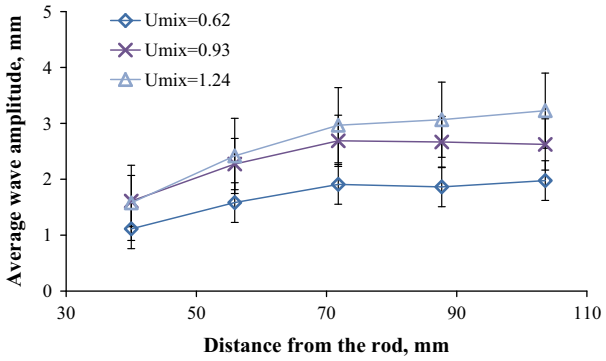

Fig. 12. Effect of mixture velocity on average wave amplitudes at different distances from the bluff body for $r = 1$.

in wavelength over distance was less than 1 mm and the standard deviation was less than 3% for all flow conditions, apart from $U_{mix} = 0.78$ m/s, $r = 0.67$, where the standard deviation was 6.5% on average. In previous studies without a bluff body an increase in wavelength was accompanied by a decrease in wave amplitude [8,58,17,59,18]. In the current study, however, the wavelengths remained almost constant while the wave amplitudes increased with distance.

The results indicate a complex system. In case of unbounded flows, this system involves two main different types of instabilities. At the inlet, a single shear layer between the fluids leads to a convective instability (KH instability) while a double shear layer leads to an absolute instability (vortex shedding behind the wake of the cylinder; Huerre and Monkewitz [60]). It is believed that the wave amplitude is increased as a result of the synergy between the two types of instabilities. However, the coupling of these instabilities is not well understood, particularly for wall bounded flows [61,62] and would require further work.

3.2.3. Average wave frequency

The average frequency of the waves generated behind the bluff body at different distances away from the rod is given in Fig. 14. For all 7 conditions investigated, the wave frequencies did not vary significantly with distance. The small fluctuations in the values at the higher mixture velocities were less than 4%. The wave frequencies increased with increasing mixture velocity. The input ratio, however, did not have any significant effect as can be seen from the two cases of $U_{mix} = 0.78$ and 1.09 m/s, where different input ratios were studied. The wave frequencies were also studied with the double-wired conductance probe for the few conditions where there were no drops present. There is good agreement with the results from the high speed imaging with frequency peaks at 26 Hz and 33 Hz for mixture velocities of 0.62 m/s and 0.78 m/s respectively.

From the measured wave frequencies the Strouhal number was calculated using the actual water velocity computed based on the average interface height. The mean value for the 7 flow conditions investigated was 0.24 with 9% standard deviation. This number is in good agreement with the literature value of 0.2 for vortex shedding behind a cylinder in single phase unbounded flows. The agreement suggests that the interfacial waves are caused by the von Karman vortices generated by the rod. The agreement was good even for the cases where small KH waves formed at the inlet for r different than 1. It seems that, at least for the flow conditions studied, vortices generated by the rod dominated over the KH waves. In addition, the pipe wall does not affect the vortex frequencies. The distance between the rod and the pipe wall varies from 0 to 6.75 mm measured along the cylinder from the bottom of the pipe. It has been shown that vortices can be suppressed

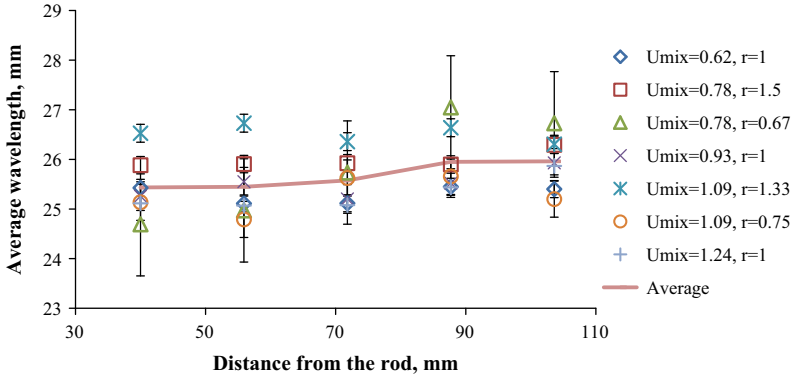

Fig. 13. Average wavelength at different distances behind the bluff body for all flow conditions investigated.

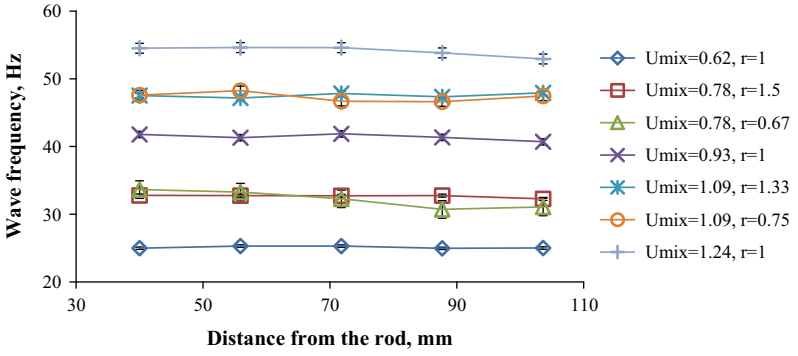

Fig. 14. Average wave frequency at different distances behind the bluff body for all flow conditions investigated.

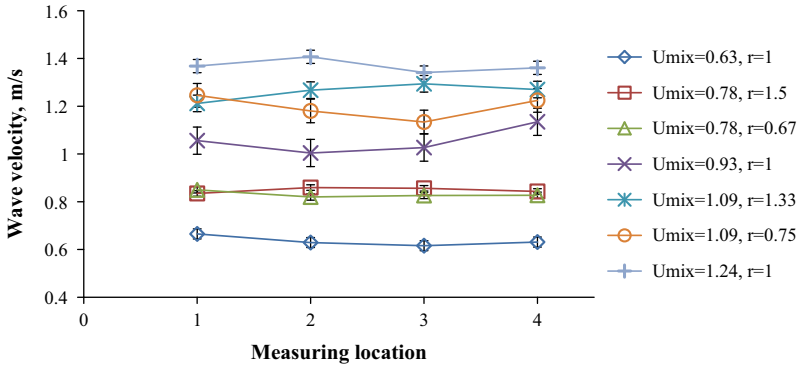

Fig. 15. Average wave velocity at different distances behind the bluff body for all flow conditions investigated.

when the ratio of the distance between the wall and the cylinder over the size of the cylinder is smaller than 0.3 [46]. For the current system only 9.8% of the length of the rod falls below this critical ratio. However, further investigations of the velocity fields would be required to fully understand the flow behind the bluff body in this configuration and its interactions with the interface.

3.2.4. Average wave velocity

Average wave velocities for the different conditions investigated are shown in Fig. 15. The wave velocities increase with mixture velocity and do not vary significantly with distance from the rod especially at the lower mixture velocities. At the higher mixture velocities, there are more fluctuations with maximum deviation of about 4% from the mean value. In the current work, for all conditions investigated the wave velocities were 9.6% faster than the mixture velocity on average regardless of the input flowrates. Other studies [18,59,63] also reported that the wave velocity was different from the mixture velocity. It is possible that these differences are due to the different mechanism of the generation of the waves; waves observed in previous studies resulted from a KH instability that depends on the velocity difference between the two phases at the inlet, whereas in the current study the waves seem to result predominantly from the vorticies shed by the bluff body. In addition, the blockage caused by the bluff body leads to a local acceleration of the fluid below and above the cylinder and it is possible that this affects the wave velocity.

4. Conclusions

In this paper the effect of a cylindrical bluff body placed inside a pipe to the flow patterns and interface characteristics of a two-phase liquid–liquid system were studied experimentally, using high speed imaging and a conductance probe. The aim was to passively actuate waves in the interface and the transition from stratified to non-stratified flows. It was found that the rod reduced the transition to lower mixture velocities while the change in flow patterns persisted at 7 m downstream the rod. In stratified flows the bluff body generated interfacial waves attributed to the interactions of the von Karman vortices in the wake of the rod with the oil–water interface.

An increase in interface height was seen after the rod that was affected by both the mixture velocity and the input ratio of the phase flowrates. The average wave amplitude increased with distance from the rod, while the average wavelength and frequency remained almost constant. The Strouhal number agreed with the literature value of 0.2 for vortex shedding behind a cylinder in single phase flows with no wall present. The wave velocities were found to be about 10% higher than the mixture velocity. Further investigations of the velocity fields in the water phase are needed to reveal the interactions between the vortices shed by the rod and the liquid–liquid interface.

Although the current investigations are at their initial stage, the use of bluff bodies in multiphase flows in pipes promises to have many important industrial applications. The presence of a bluff body in a pipe can enhance two-phase mixing and improve mass and heat transfer rates; the current approach can therefore be used in heat exchangers and in mixing processes. In addition, the use of a bluff body can improve the overall control of the flow patterns inside pipes, for example during transportation of oil–water mixtures, important for flow assurance applications.

Acknowledgements

The project was supported by the EPSRC Programme Grant MEMPHIS. K. H. Park would like to acknowledge UCL for providing his studentship. The authors would also like to acknowledge the EPSRC Instrument Pool for the loan of the high speed camera Photron SA-1.

References

[1] N. Brauner, D.M. Maron, Flow pattern transitions in two-phase liquid–liquid flow in horizontal tubes, Int. J. Multiph. Flow 18 (1) (1992) 123–140.
[2] N. Brauner, D.M. Maron, Stability analysis of stratified liquid–liquid flow, Int. J. Multiph. Flow 18 (1) (1992) 103–121.
[3] N. Brauner, D. MoalemMaron, Classification of liquid–liquid two-phase flow systems and the prediction of flow pattern maps, in: 2nd International Symposium on Two-Phase Flow Modeling and Experimentation – ISTP, vol. 99, 1999, pp. 747–754.
[4] N. Brauner, The prediction of dispersed flows boundaries in liquid–liquid and gas–liquid systems, Int. J. Multiph. Flow 27 (5) (2001) 885–910.
[5] A.C. Bannwart, O.M. Rodriguez, C.H. de Carvalho, I.S. Wang, R.M. Vara, Flow patterns in heavy crude oil–water flow, J. Energy Res. Technol. 126 (3) (2004) 184–189.
[6] T. Al-Wahaibi, M. Smith, P. Angeli, Transition between stratified and non-stratified horizontal oil–water flows. Part II: Mechanism of drop formation, Chem. Eng. Sci. 62 (11) (2007) 2929–2940.
[7] T. Al-Wahaibi, N. Yusuf, Y. Al-Wahaibi, A. Al-Ajmi, Experimental study on the transition between stratified and non-stratified horizontal oil–water flow, Int. J. Multiph. Flow 38 (1) (2012) 126–135.
[8] J.L. Trallero, Oil–Water Flow Patterns in Horizontal Pipes, University of Tulsa Fluid Flow Projects, 1995.
[9] D. Barnea, Y. Taitel, Kelvin–Helmholtz stability criteria for stratified flow: viscous versus non-viscous (inviscid) approaches, Int. J. Multiph. Flow 19 (4) (1993) 639–649.
[10] T. Al-Wahaibi, P. Angeli, Transition between stratified and non-stratified horizontal oil–water flows. Part I: Stability analysis, Chem. Eng. Sci. 62 (11) (2007) 2915–2928.
[11] R.V.A. Oliemans, The Lubricating-Film Model for Core-Annular Flow, PhD Thesis, Delft University, The Netherlands, 1986.
[12] R. Bai, Traveling Waves in a High Viscosity Ratio and Axisymmetric Core Annular Flow, Ph.D. Thesis, Faculty of the Graduate School, University of Minnesota, 1995.
[13] A.C. Bannwart, Wavespeed and volumetric fraction in core annular flow, Int. J. Multiph. Flow 24 (6) (1998) 961–974.

[14] R. Bai, D.D. Joseph, Steady flow and interfacial shapes of a highly viscous dispersed phase, Int. J. Multiph. Flow 26 (9) (2000) 1469–1491.
[15] O.M.H. Rodriguez, A.C. Bannwart, Analytical model for interfacial waves in vertical core flow, J. Petrol. Sci. Eng. 54 (3) (2006) 173–182.
[16] O.M.H. Rodriguez, A.C. Bannwart, Experimental study on interfacial waves in vertical core flow, J. Petrol. Sci. Eng. 54 (3) (2006) 140–148.
[17] T. Al-Wahaibi, P. Angeli, Experimental study on interfacial waves in stratified horizontal oil–water flow, Int. J. Multiph. Flow 37 (8) (2011) 930–940.
[18] A.H. Barral, A. Ebenezer, P. Angeli, Investigations of interfacial waves at the inlet section in stratified oil–water flows, Exp. Therm. Fluid Sci. 60 (2015) 115–122.
[19] J.H. Duncan, An experimental investigation of breaking waves produced by a towed hydrofoil, Proceedings of the Royal Society of London A: Mathematical, Physical and Engineering Sciences, vol. 377, The Royal Society, 1981, pp. 331–348 (No. 1770).
[20] J.H. Duncan, The breaking and non-breaking wave resistance of a two-dimensional hydrofoil, J. Fluid Mech. 126 (1983) 507–520.
[21] E. Berger, R. Wille, Periodic flow phenomena, Annu. Rev. Fluid Mech. 4 (1) (1972) 313–340.
[22] J.T. Lin, Y.H. Pao, Wakes in stratified fluids, Annu. Rev. Fluid Mech. 11 (1) (1979) 317–338.
[23] P.W. Bearman, Vortex shedding from oscillating bluff bodies, Annu. Rev. Fluid Mech. 16 (1) (1984) 195–222.
[24] H. Oertel Jr, Wakes behind blunt bodies, Annu. Rev. Fluid Mech. 22 (1) (1990) 539–562.
[25] O.M. Griffin, M.S. Hall, Review—vortex shedding lock-on and flow control in bluff body wakes, J. Fluids Eng. 113 (4) (1991) 526–537.
[26] M. Coutanceau, J.R. Defaye, Circular cylinder wake configurations: a flow visualization survey, Appl. Mech. Rev. 44 (6) (1991) 255–305.
[27] C.H. Williamson, Vortex dynamics in the cylinder wake, Annu. Rev. Fluid Mech. 28 (1) (1996) 477–539.
[28] C.H.K. Williamson, Three-dimensional wake transition, J. Fluid Mech. 328 (1996) 345–407.
[29] M.M. Zdravkovich, Flow around circular cylinders; Vol. I: Fundamentals, J Fluid Mech 350 (1) (1997) 377–378.
[30] J.C. Lin, D. Rockwell, Evolution of a quasi-steady breaking wave, J. Fluid Mech. 302 (1995) 29–44.
[31] S. Malavasi, A. Guadagnini, Hydrodynamic loading on river bridges, J Hydraul Eng 129 (11) (2003) 854–861.
[32] S. Malavasi, A. Guadagnini, Interactions between a rectangular cylinder and a free-surface flow, J. Fluids Struct. 23 (8) (2007) 1137–1148.
[33] S. Malavasi, S. Franzetti, G. Blois, PIV investigation of flow around submerged river bridge deck, in: Proceedings of the International Conference of River Flows, Napoli, Italy, June 2004, pp. 601–608.
[34] H. Miyata, N. Shikazono, M. Kanai, Forces on a circular cylinder advancing steadily beneath the free-surface, Ocean Eng. 17 (1) (1990) 81–104.
[35] J. Sheridan, J.C. Lin, D. Rockwell, Flow past a cylinder close to a free surface, J. Fluid Mech. 330 (1997) 1–30.
[36] J. Carberry, J. Sheridan, D. Rockwell, Forces and wake modes of an oscillating cylinder, J. Fluids Struct. 15 (3) (2001) 523–532.
[37] J. Carberry, J. Sheridan, D. Rockwell, Controlled oscillations of a cylinder: forces and wake modes, J. Fluid Mech. 538 (2005) 31–69.
[38] P. Reichl, K. Hourigan, M.C. Thompson, Flow past a cylinder close to a free surface, J. Fluid Mech. 533 (2005) 269–296.
[39] P.W. Bearman, M.M. Zdravkovich, Flow around a circular cylinder near a plane boundary, J. Fluid Mech. 89 (01) (1978) 33–47.
[40] G. Buresti, A. Lanciotti, Vortex shedding from smooth and roughened cylinders in cross-flow near a plane surface, Aeronaut. Quart. 30 (1979) 305–321.
[41] F. Angrilli, S. Bergamaschi, V. Cossalter, Investigation of wall induced modifications to vortex shedding from a circular cylinder, J. Fluids Eng. 104 (4) (1982) 518–522.
[42] A.J. Grass, P.W.J. Raven, R.J. Stuart, J.A. Bray, The influence of boundary layer velocity gradients and bed proximity on vortex shedding from free spanning pipelines, J. Energy Res. Technol. 106 (1) (1984) 70–78.
[43] S. Taniguchi, K. Miyakoshi, Fluctuating fluid forces acting on a circular cylinder and interference with a plane wall, Exp. Fluids 9 (4) (1990) 197–204.
[44] C. Lei, L. Cheng, K. Kavanagh, Re-examination of the effect of a plane boundary on force and vortex shedding of a circular cylinder, J. Wind Eng. Ind. Aerodyn. 80 (3) (1999) 263–286.
[45] S.J. Price, D. Sumner, J.G. Smith, K. Leong, M.P. Paidoussis, Flow visualization around a circular cylinder near to a plane wall, J. Fluids Struct. 16 (2) (2002) 175–191.
[46] X.K. Wang, S.K. Tan, Near-wake flow characteristics of a circular cylinder close to a wall, J. Fluids Struct. 24 (5) (2008) 605–627.
[47] J.H. Chen, W.G. Pritchard, S.J. Tavener, Bifurcation for flow past a cylinder between parallel planes, J. Fluid Mech. 284 (1995) 23–41.
[48] L.A. Jurman, S.E. Deutsch, M.J. McCready, Interfacial mode interactions in horizontal gas—liquid flows, J. Fluid Mech. 238 (1992) 187–219.
[49] B.J. Azzopardi, Drops in annular two-phase flow, Int. J. Multiph. Flow 23 (1997) 1–53.
[50] T.S. Ng, Interfacial Structure of Stratified Pipe Flow, Ph.D. Thesis, Imperial College, University of London, 2002.
[51] Z. Wang, K.S. Gabriel, D.L. Manz, The influences of wave height on the interfacial friction in annular gas–liquid flow under normal and microgravity conditions, Int. J. Multiph. Flow 30 (10) (2004) 1193–1211.
[52] A.K. Jana, G. Das, P.K. Das, Flow regime identification of two-phase liquid–liquid upflow through vertical pipe, Chem. Eng. Sci. 61 (5) (2006) 1500–1515.
[53] U. Kadri, R.F. Mudde, R.V.A. Oliemans, M. Bonizzi, P. Andreussi, Prediction of the transition from stratified to slug flow or roll-waves in gas–liquid horizontal pipes, Int. J. Multiph. Flow 35 (11) (2009) 1001–1010.
[54] A.H. Barral, P. Angeli, Interfacial characteristics of stratified liquid–liquid flows using a conductance probe, Exp. Fluids 54 (10) (2013) 1–15.
[55] A.H. Barral, L.C. Edomwonyi-Otu, P. Angeli, Flow patterns and interfacial characteristics in stratified oil–water flows in pipes of different diameter, in: Experimental Methods in Multiphase Flows, Jeju, South Korea, 2013, pp. 1–6.
[56] J.R. Chaplin, Nonlinear forces on a horizontal cylinder beneath waves, J. Fluid Mech. 147 (1984) 449–464.
[57] A.A. Dimas, Free-surface waves generation by a fully submerged wake, Wave Motion 27 (1) (1998) 43–54.
[58] T. Al-Wahaibi, Investigations on the Transition between Stratified to Non-Stratified Horizontal Oil–Water Flows, Ph.D. Thesis, University College London, 2006.
[59] M.S. de Castro, C.C. Pereira, J.N. Dos Santos, O.M. Rodriguez, Geometrical and kinematic properties of interfacial waves in stratified oil–water flow in inclined pipe, Exp. Therm. Fluid Sci. 37 (2012) 171–178.
[60] P. Huerre, P.A. Monkewitz, Local and global instabilities in spatially developing flows, Annu. Rev. Fluid Mech. 22 (1) (1990) 473–537.
[61] J.M. Chomaz, Global instabilities in spatially developing flows: non-normality and nonlinearity, Annu. Rev. Fluid Mech. 37 (2005) 357–392.
[62] P. Gondret, P. Ern, L. Meignin, M. Rabaud, Experimental evidence of a nonlinear transition from convective to absolute instability, Phys. Rev. Lett. 82 (7) (1999) 1442.
[63] M.S. de Castro, O.M. Rodriguez, Interfacial waves in stratified viscous oil–water flow, Exp. Therm. Fluid Sci. 62 (2015) 85–98.